Supporting Information

Negative Electron Affinity Driven Broadband Absorption of $Cs_{3+n}Pb_nSb_2I_{9+3n}$/GaN van der Waals Heterostructures

Xiao-dong Yang,[a, b] *Hai-bo Shu,*[*, c] *Xin-xin Wang,*[a, b] *Yang Shen,*[*, c] *Nai-feng Shen,*[a, b, d] *Bao-lin Wang,*[e] *Jian-guo Wan*[*, a, b] *and Guang-hou Wang,*[a, b]

[a]National Laboratory of Solid State Microstructures, Department of Physics, Nanjing University, Nanjing 210093, P. R. China. E-mail: wanjg@nju.edu.cn

[b]Collaborative Innovation Center of Advanced Microstructures, Nanjing University, Nanjing 210093, P. R. China

[c]College of Optical and Electronic Technology, China Jiliang University, 310018 Hangzhou, China

[d]First-class Disciplinesans and High-level University Construction Office, Nanjing University of Posts and Telecommunications, Nanjing 210023, P. R. China

[e]College of Physical Science and Technology, Nanjing Normal University, Nanjing 210023, P. R. China

Corresponding Author

*E-mail: shu123hb@gmail.com

*E-mail: wanjg@nju.edu.cn

Section S1. Test of the convergence of cutoff energy

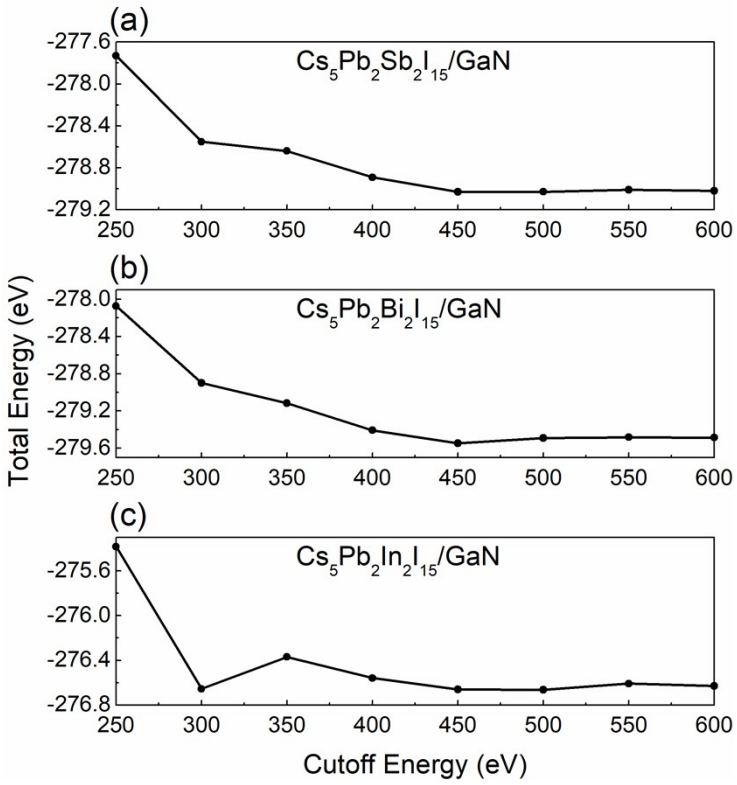

Fig. S1. Total energies of (a) $Cs_5Pb_2Sb_2I_{15}$/GaN, (b) $Cs_5Pb_2Bi_2I_{15}$/GaN, and (c) $Cs_5Pb_2In_2I_{15}$/GaN heterostructure as a function of cutoff energy.

Table S1. Energy convergence test of $Cs_{3+n}Pb_nSb_2I_{9+3n}$/GaN, $Cs_{3+n}Pb_nBi_2I_{9+3n}$/GaN and $Cs_{3+n}Pb_nIn_2I_{9+3n}$/GaN heterostructures in their PGA-2 structures (n = 2), respectively. E_{pe} is the total energy per atom of MHP/GaN heterostructures and ΔE_{pe} is the difference of the total energy per atom between two neighbouring test points.

cutoff energy	$Cs_{3+n}Pb_nSb_2I_{9+3n}$/GaN		$Cs_{3+n}Pb_nBi_2I_{9+3n}$/GaN		$Cs_{3+n}Pb_nIn_2I_{9+3n}$/GaN	
	E_{pe} (eV/atom)	ΔE_{pe} (meV/atom)	E_{pe} (eV/atom)	ΔE_{pe} (meV/atom)	E_{pe} (eV/atom)	ΔE_{pe} (meV/atom)
250 eV	-4.208032	--	-4.213221	--	-4.172461	--

300 eV	-4.220490	-12.458	-4.225734	-12.513	-4.191745	-19.284
350 eV	-4.221806	-1.316	-4.229029	-3.295	-4.187411	4.334
400 eV	-4.225630	-3.824	-4.233440	-4.411	-4.190283	-2.872
450 eV	-4.227739	-2.109	-4.235553	-2.113	-4.191826	-1.543
500 eV	-4.227707	0.032	-4.234690	0.863	-4.191882	-0.056
550 eV	-4.227421	0.286	-4.234573	0.117	-4.191044	0.838
600 eV	-4.227592	-0.171	-4.234621	-0.048	-4.191350	-0.306

Section S2. The calculated band gaps (E_g) of $CsPbI_3$ and GaN using different methods

Table S2. The band gaps of $CsPbI_3$ and GaN calculated using different methods. For the comparison, previous reports on the band gaps of $CsPbI_3$ and GaN were also listed here.

E_g (eV)	PBE	PBE+SOC	HSE06+SOC	Previous works
$CsPbI_3$	1.449	1.227	1.701	1.67[1], 1.73[2]
GaN	1.622	1.439	3.394	3.39[3], 3.47[4]

Section S3. Surface energies of 2D $Cs_4PbM_2I_{12}$ (M= Pb, Sb, In and Bi) nanosheets

In order to evaluate the surface stability of 2D $Cs_4PbM_2I_{12}$ (M= Pb, Sb, In and Bi) nanosheets, their relative surface energies (γ_s) were calculated as follows

$$\gamma_s = (E_T - n_v E_{CsPbI_3} + \sum_i \Delta n_i \mu_i)/2A \quad \text{(S1)}$$

where E_T and E_{CsPbI_3} are total energies of 2D $Cs_4PbM_2I_{12}$ nanosheets and $CsPbI_3$ in cubic bulk, respectively. A is the surface area of nanosheets, n_v is the number of $CsPbI_3$ formula unit in 2D nanosheets, μ_i is the chemical potential of atomic species i (i = Pb, Sb, In and Bi), and Δn_i is the difference of atom numbers between the given 2D structure and n_v bulk $CsPbI_3$. As listed in Table S3, calculated surface energies of $Cs_4PbM_2I_{12}$ (M= Pb, Sb, In and Bi) nanosheets are 44.39, -20.84, 36.44 and 39.63 meV/Å^2, respectively. The result suggests that the introduction of trivalent cations M (M = Sb, In and Bi) onto the surface layers of 2D $CsPbI_3$ nanosheets can leads to the reduction of surface energies, which contributes to the stability of 2D $CsPbI_3$ nanosheets.

Table S3. Surface energies (γ_s) of $Cs_4PbM_2I_{12}$ (M= Pb, Sb, In and Bi) nanosheets.

	$Cs_4Pb_3I_{12}$	$Cs_4PbSb_2I_{12}$	$Cs_4PbIn_2I_{12}$	$Cs_4PbBi_2I_{12}$
γ_s (eV/Å^2)	44.39	-20.84	36.44	39.63

Section S4. Band structures of 2D $Cs_4PbM_2I_{12}$ (M= Pb, Bi, In and Sb) nanosheets

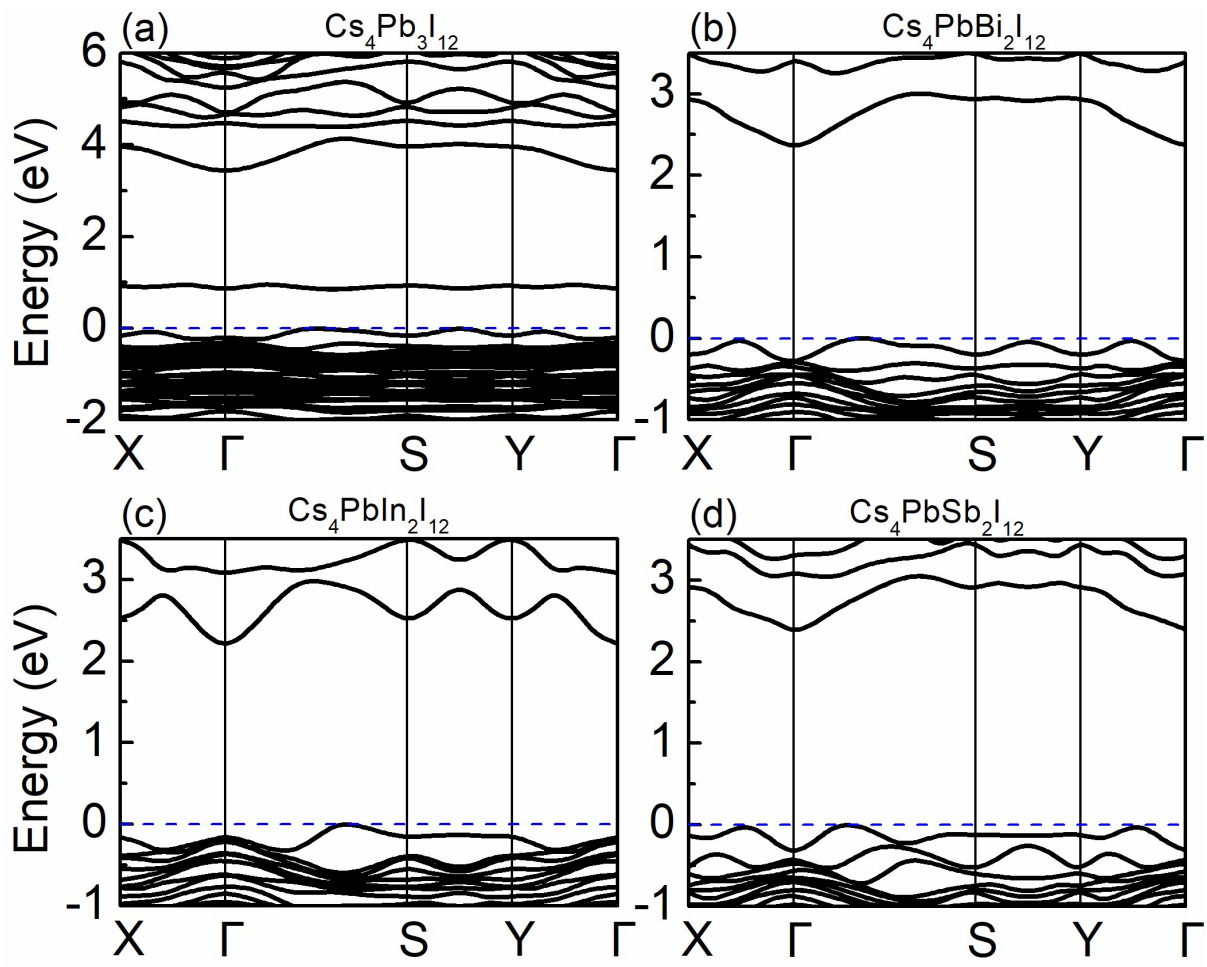

Fig. S2. Band structures of (a) pristine $CsPbI_3$ thin nanosheet, $CsPbI_3$ thin nanosheets saturated by (b) Bi^{3+}, (c) In^{3+} and (d) Sb^{3+} cations, respectively. The zero of the Fermi energy is set at VBM.

Section S5. Partial charge-density distributions of $Cs_4PbSb_2I_{12}$ nanosheets

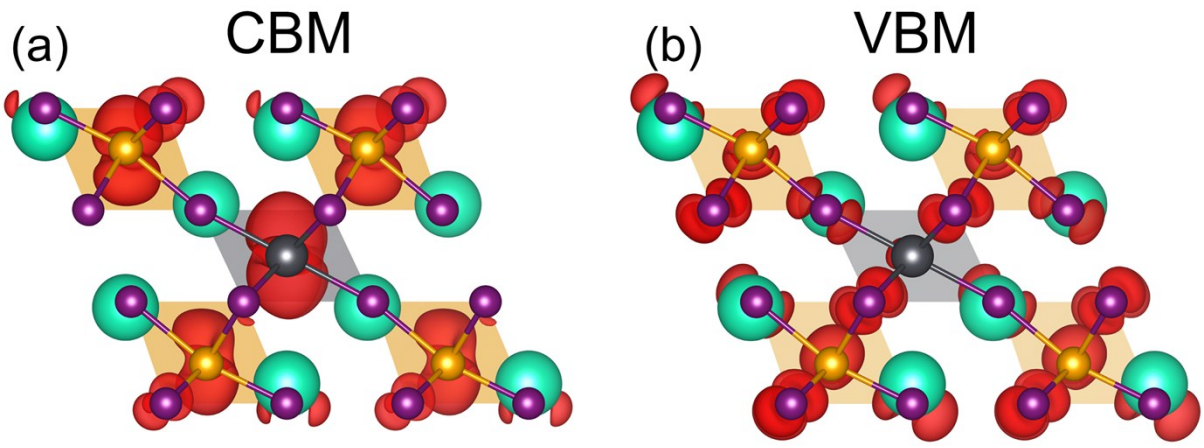

Fig. S3. Charge-density distributions of (a) CBM and (b) VBM of $Cs_4PbSb_2I_{12}$ nanosheet.

Section S6. Interfacial configurations of heterostructures

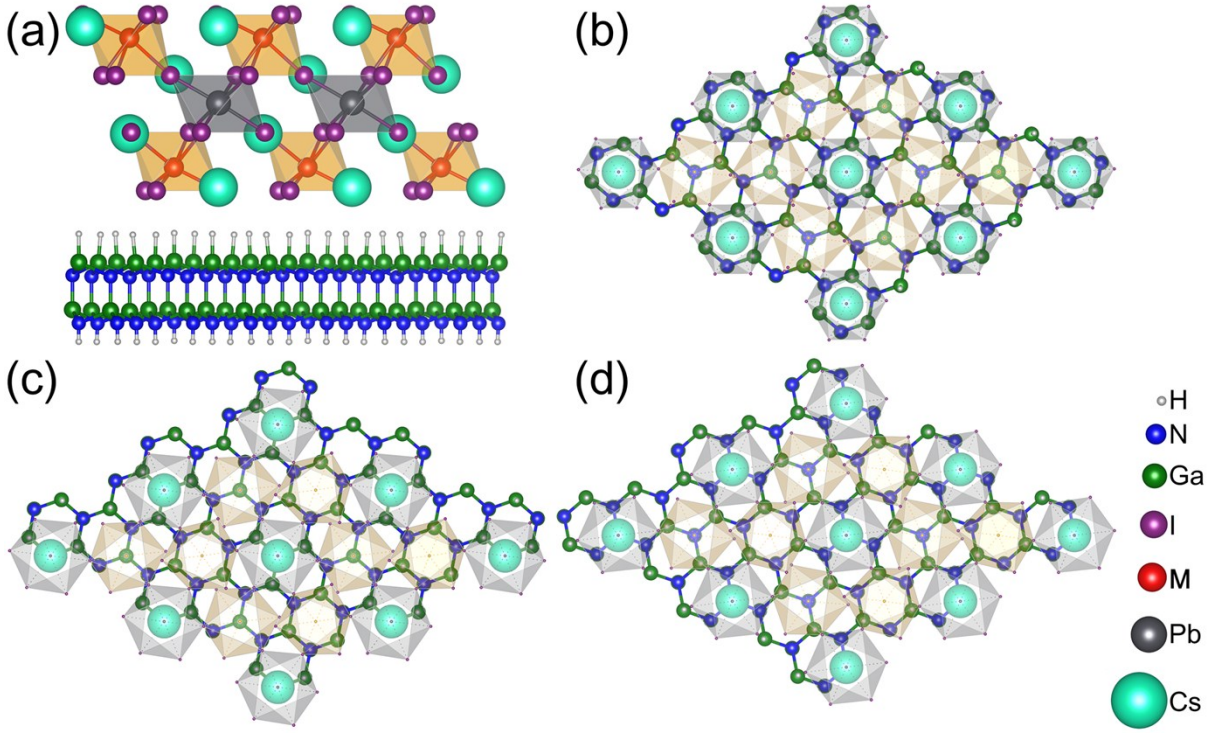

Fig. S4. (a) Side view of atomic structure of $Cs_{3+n}Pb_nM_2I_{9+3n}$/GaN heterostructure (M = Sb, In and Bi, n = 1). Top view of atomic structures of $Cs_4PbM_2I_{12}$/GaN heterostructure (M = Sb, In and Bi) with (b) hollow, (c) N-top, and (d) Ga-top interfacial configurations. Cs, I, Ga, N and H atoms are shown in cyan, purple, green, blue and white, respectively. Sb-I and Pb-I polyhedral are colored by orange and black, respectively. The red spheres represent to the trivalent cations, such as Sb^{3+}, In^{3+} and Bi^{3+}, located at the surface of perovskite layer in the heterostructure.

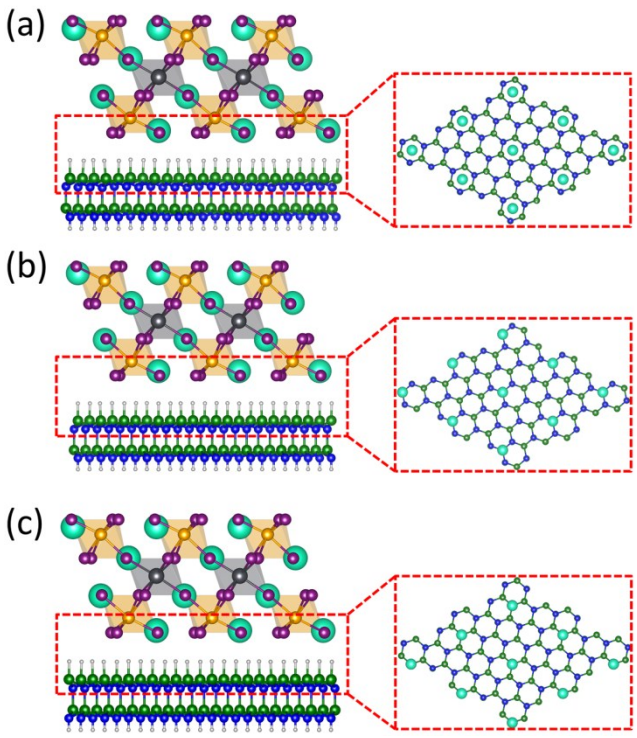

Fig. S5. Side view of atomic structures of $Cs_4PbSb_2I_{12}$/GaN(0001) heterostructure (PGA-2) with (a) hollow, (b) Ga-top, and (c) N-top interfacial configurations. The insets indicate the corresponding interface atomic configurations.

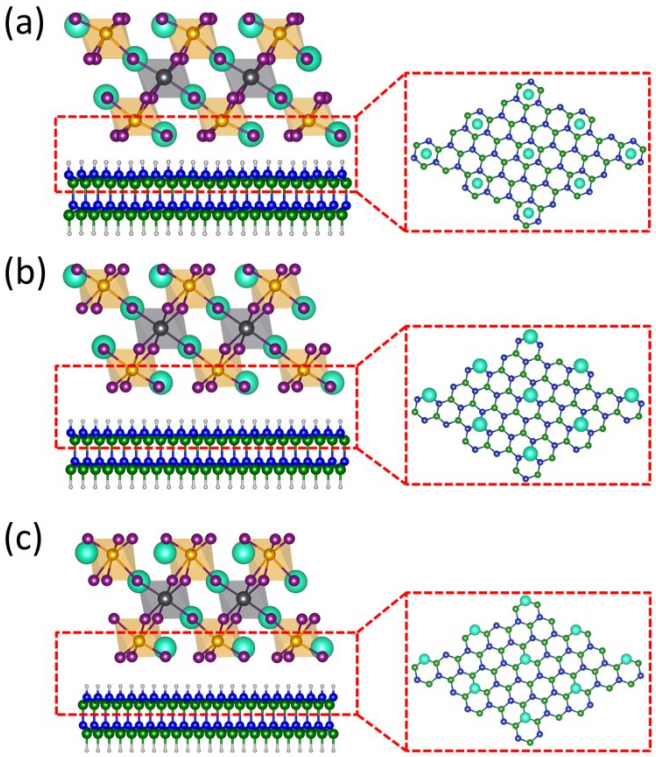

Fig. S6. Side view of atomic structures of $Cs_4PbSb_2I_{12}$/GaN(000$\bar{1}$) heterostructure (PGB-1)

with (a) hollow, (b) Ga-top, and (c) N-top interfacial configurations. The insets indicate the corresponding interface atomic configurations.

Table S4. Interlayer distance *d* of $Cs_4PbSb_2I_{12}$/GaN, $Cs_4PbIn_2I_{12}$/GaN, and $Cs_4PbBi_2I_{12}$/GaN heterostructures with three different configurations.

Heterostructure	Configuration	Interlayer distance *d* (Å)
$Cs_4PbSb_2I_{12}$/GaN	Hollow	2.903
	Ga-top	3.051
	N-top	2.956
$Cs_4PbIn_2I_{12}$/GaN:	Hollow	2.887
	Ga-top	3.065
	N-top	3.056
$Cs_4PbBi_2I_{12}$/GaN	Hollow	2.814
	Ga-top	3.028
	N-top	3.088

Section S7. Elastic stiffness constants and stability of heterostructures

The elastic stiffness constants C_{ij} are important parameters to evaluate the structural stability of $Cs_{3+n}Pb_nM_2I_{9+3n}$/GaN heterostructures (M = Sb, In and Bi). Taking $Cs_4PbM_2I_{12}$/GaN heterostructures (M = Sb, In and Bi) as an example, all of them have a monoclinic symmetry, resulting in thirteen independent elastic constants as follows

$$C = \begin{pmatrix} C_{11} & C_{12} & C_{13} & 0 & 0 & C_{16} \\ C_{21} & C_{22} & C_{23} & 0 & 0 & C_{26} \\ C_{31} & C_{32} & C_{33} & 0 & 0 & C_{36} \\ 0 & 0 & 0 & C_{44} & C_{45} & 0 \\ 0 & 0 & 0 & C_{45} & C_{55} & 0 \\ C_{16} & C_{26} & C_{36} & 0 & 0 & C_{66} \end{pmatrix} \quad \text{(S2)}$$

For a monoclinic crystal, the criteria for mechanical stability were given by the following equations[5]:

$$C_{11} > 0,\ C_{22} > 0,\ C_{33} > 0,\ C_{44} > 0,\ C_{55} > 0,\ C_{66} > 0,$$

$$[C_{11} + C_{22} + C_{33} + 2(C_{12} + C_{13} + C_{23})] > 0,$$

$$(C_{33}C_{55} - C_{35}^2) > 0,\ (C_{44}C_{66} - C_{46}^2) > 0,\ (C_{22}C_{33} - 2C_{23}) > 0,$$

$$[C_{22}(C_{33}C_{55} - C_{35}^2) + 2C_{23}C_{25}C_{35} - C_{23}^2C_{55} - C_{25}^2C_{33}] > 0,$$

$$\{2[C_{15}C_{25}(C_{33}C_{12} - C_{13}C_{23}) + C_{15}C_{35}(C_{22}C_{13} - C_{12}C_{23}) + C_{25}C_{35}(C_{11}C_{23} - C_{12}C_{13})]$$

$$- [C_{15}^2(C_{22}C_{33} - C_{23}^2) + C_{25}^2(C_{11}C_{33} - C_{13}^2) + C_{35}^2(C_{11}C_{22} - C_{12}^2)] + C_{55}g\} > 0$$

$$g = C_{11}C_{22}C_{33} - C_{11}C_{23}^2 - C_{22}C_{13}^2 - C_{33}C_{12}^2 + 2C_{12}C_{13}C_{23}. \quad \text{(S3)}$$

The calculated elastic constants of $Cs_4PbM_2I_{12}$/GaN heterostructures (M = Sb, In and Bi) were listed in Table S5. Based on the criteria of mechanical stability, we find that only the hollow configuration of $Cs_4PbSb_2I_{12}$/GaN heterostructures is mechanically stable, while the Ga-top and N-top configurations are unstable. Similarly, the Ga-top and N-top configurations of $Cs_4PbIn_2I_{12}$/GaN and the hollow configuration of $Cs_4PbBi_2I_{12}$/GaN heterostructure are

stable.

Table S5. Elastic stiffness constants C_{ij} and stability of $Cs_4PbM_2I_{12}$/GaN heterostructures (M = Sb, In and Bi) with different interfacial configurations.

(N/m)		C_{11}	C_{22}	C_{33}	C_{66}	C_{44}	C_{55}	C_{12}	C_{13}	C_{23}	C_{46}	C_{15}	C_{25}	C_{35}	stability
Sb^{3+}:	Hollow	105.06	105.30	30.32	26.11	11.27	7.93	38.54	14.30	9.33	0.48	3.40	-2.25	0.09	stable
	Ga-top	99.85	100.74	43.05	38.27	13.74	6.16	14.27	-4.66	0.24	0.93	21.85	18.49	4.34	unstable
	N-top	66.56	100.14	24.43	29.18	13.67	7.59	44.49	-10.12	14.31	0.76	-11.17	3.12	-6.61	unstable
In^{3+}:	Hollow	-59.55	-88.96	-51.20	-22.86	-85.90	-16.91	-138.97	-120.08	-130.25	-70.84	71.24	75.27	54.58	unstable
	Ga-top	157.87	169.66	34.51	54.38	1.75	4.63	58.61	12.40	11.14	3.74	2.44	6.87	-2.40	stable
	N-top	69.67	72.83	28.79	20.62	5.29	5.03	32.00	11.35	9.08	2.27	-1.39	-2.23	-1.71	stable
Bi^{3+}:	Hollow	122.07	127.94	34.96	38.54	16.47	14.12	49.45	14.68	13.48	-2.48	2.11	-2.51	2.64	stable
	Ga-top	178.84	173.05	-24.77	50.96	-36.11	-69.71	76.02	6.48	-15.42	-7.00	-4.57	28.54	50.44	unstable
	N-top	64.65	71.27	20.38	13.17	0.90	6.34	25.03	11.82	6.87	7.00	3.51	1.01	3.17	unstable

Section S8. Projected density of states of heterostructures

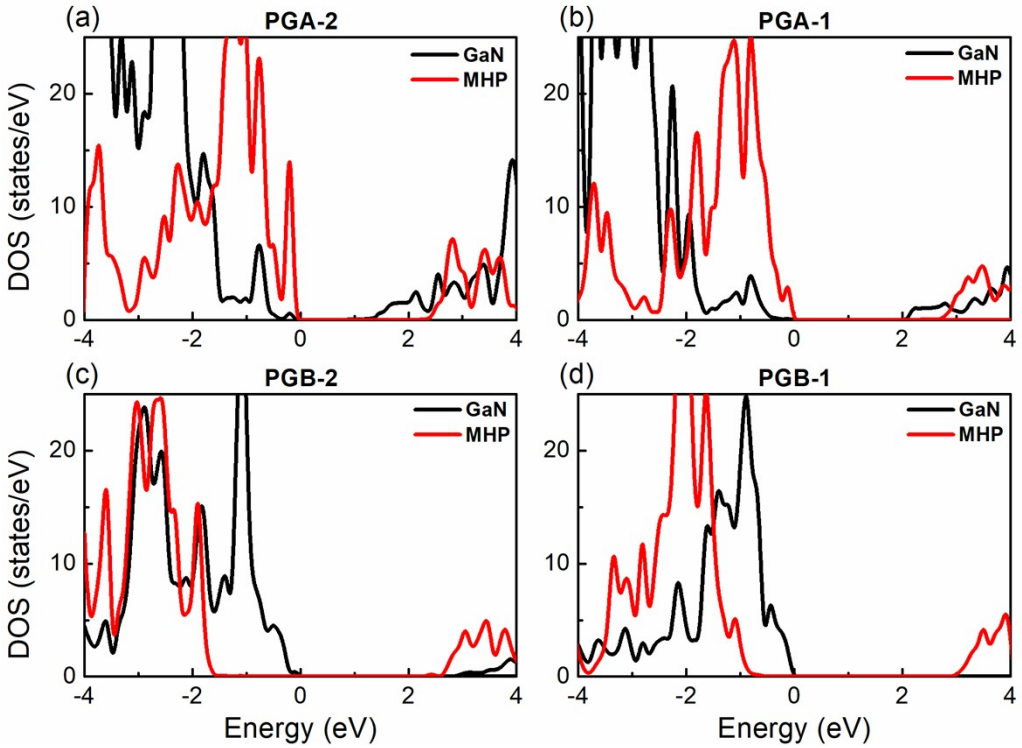

Fig. S7. Projected density of states for four different MHP/GaN heterostructures: (a) PGA-2, (b) PGA-1, (c) PGB-2, and (d) PGB-1. The red and black density of states denote the contribution of MHP and GaN sheets, respectively.

Section S9. NEA of GaN systems without and with Cs-adsorbed

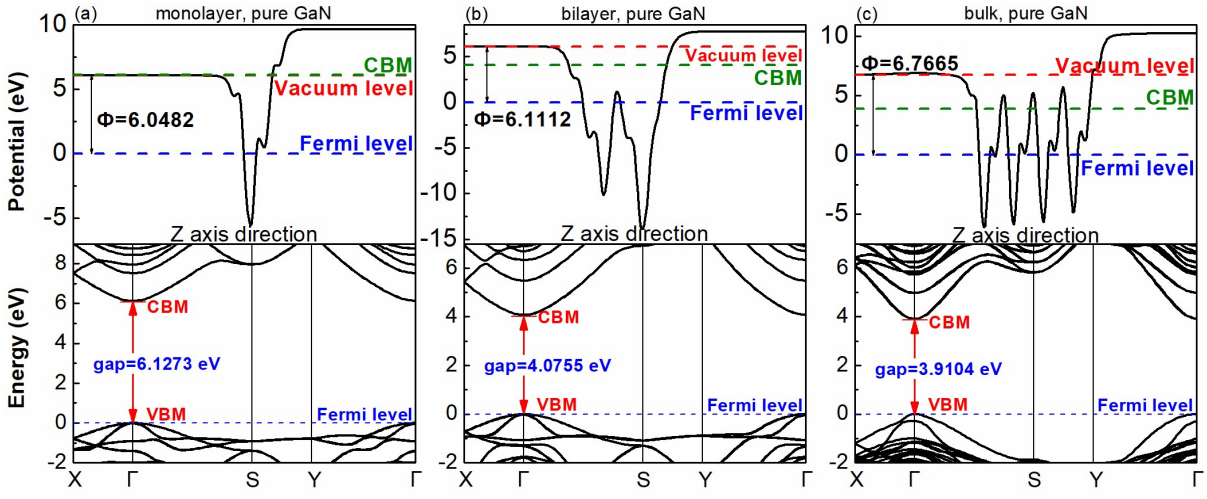

Fig. S8. Electrostatic potentials (upper panels) and band structures (lower panels) of GaN without Cs absorption in (a) monolayer, (b) bilayer and (c) bulk phase, respectively. The zero of the Fermi energy is set at VBM. Here GaN bulk is simulated by a surface slab model with six GaN bilayers and its bottom surface (N-face) are terminated by artificial hydrogen atoms with fractional charges of 0.75*e*.

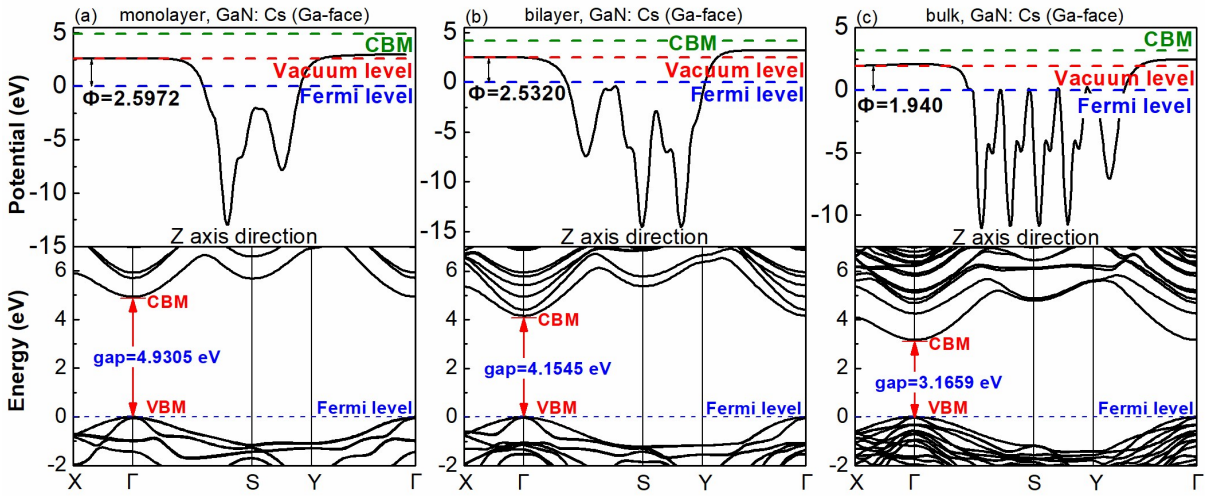

Fig. S9. Electrostatic potentials (upper panels) and band structures (lower panels) of GaN with the adsorption of Cs at Ga-face in (a) monolayer, (b) bilayer and (c) bulk phase, respectively. The zero of the Fermi energy is set at VBM. Here GaN bulk is simulated by a

surface slab model with six GaN bilayers and its bottom surface (N-face) are terminated by artificial hydrogen atoms with fractional charges of 0.75*e*.

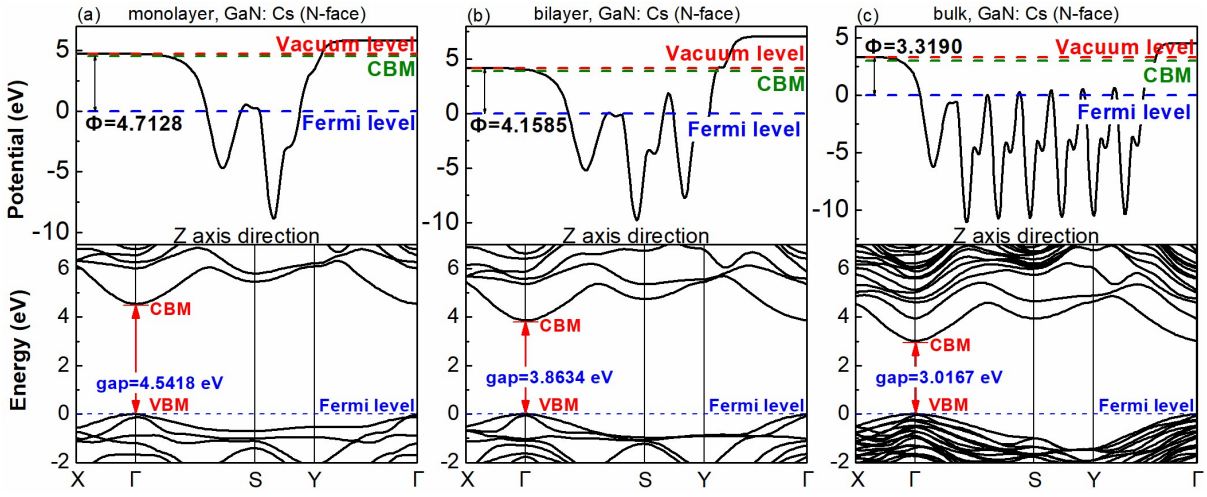

Fig. S10. Electrostatic potentials (upper panels) and band structures (lower panels) of GaN with the adsorption of Cs at N-face in (a) monolayer, (b) bilayer and (c) bulk phase, respectively. The zero of the Fermi energy is set at VBM. Here GaN bulk is simulated by a surface slab model with six GaN bilayers and its bottom surface (Ga-face) are terminated by artificial hydrogen atoms with fractional charges of 1.25*e*.

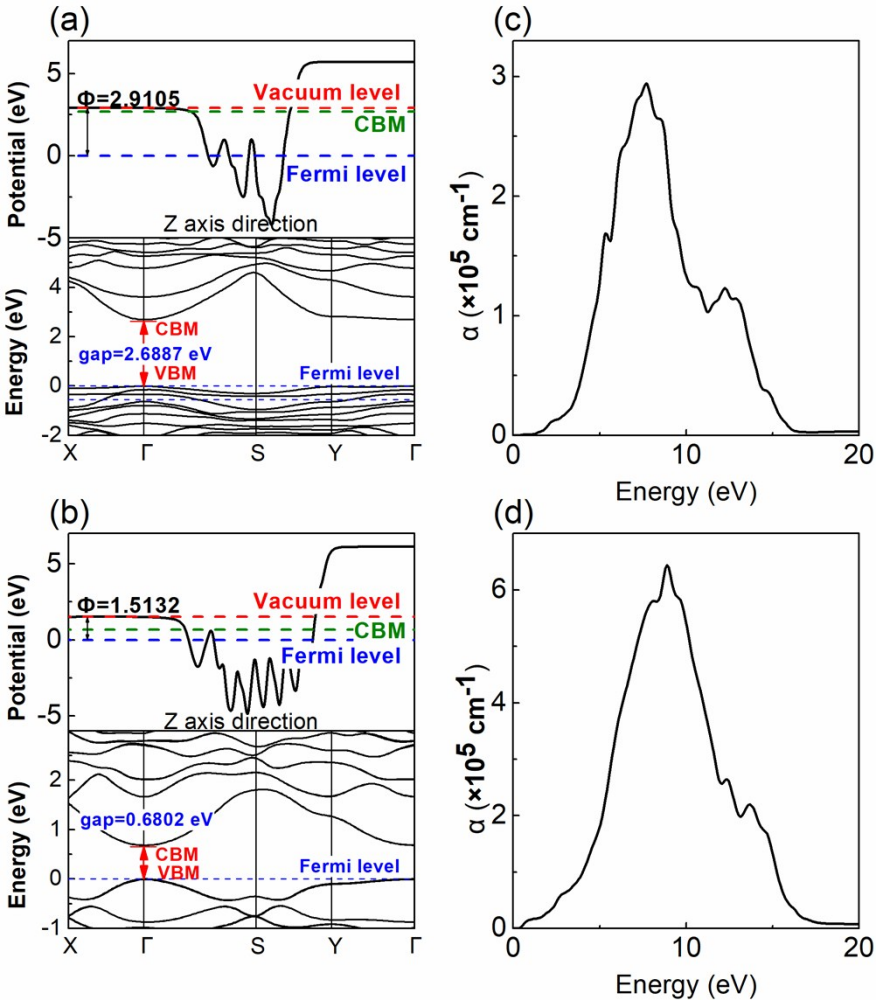

Fig. S11. Electrostatic potential distribution, band structures, and optical absorption spectra of Cs-adsorbed GaN $(11\bar{2}0)$ nanosheets. (a) Electrostatic potential (upper panel) and band structure (lower pannel) and (c) optical absorption spectrum of Cs-adsorbed trilayer GaN $(11\bar{2}0)$ nanosheet. (b) Electrostatic potential (upper panel) and band structure (lower pannel) and (d) optical absorption spectrum of Cs-adsorbed six-layer GaN $(11\bar{2}0)$ nanosheet.

Section S10. Work function and electron affinity of $Cs_4PbBi_2I_{12}$/GaN and $Cs_4PbIn_2I_{12}$/GaN heterostrutures

Table S6. Work functions (Φ) and electron affinities (χ) of 2D $Cs_4PbBi_2I_{12}$/GaN and $Cs_4PbIn_2I_{12}$/GaN heterostructures.

(eV)	$Cs_4PbBi_2I_{12}$ /GaN	$Cs_4PbIn_2I_{12}$ /GaN
Φ	1.29	1.46
χ	-0.18	-0.35

Section S11. Electronic properties of $Cs_{3+n}Pb_nSb_2I_{9+3n}$/GaN heterostructures with different *n* values

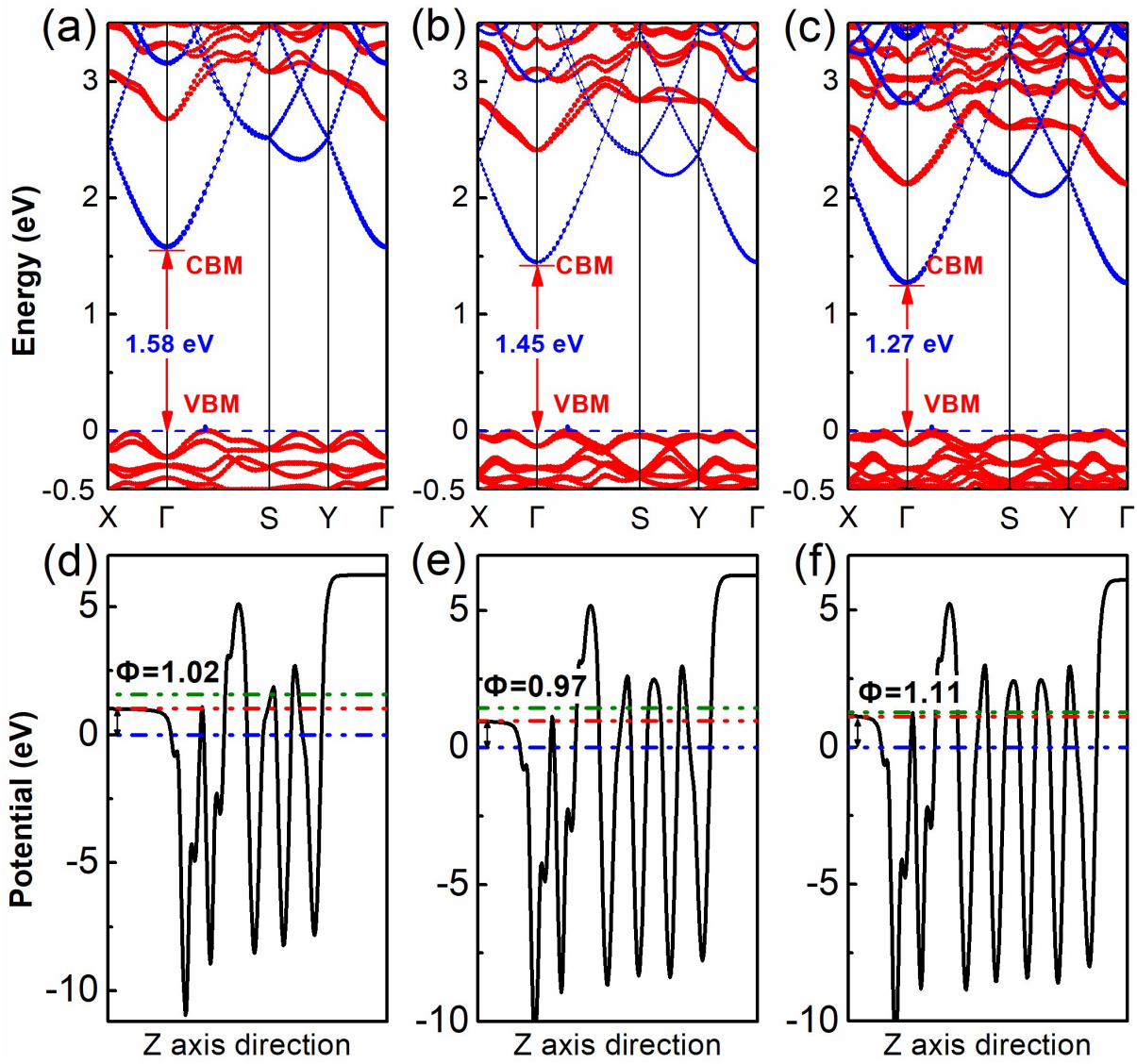

Fig. S12. Band structures and electrostatic potential distributions of $Cs_{3+n}Pb_nSb_2I_{9+3n}$/GaN heterostructures with (a, d) $n = 0$, (b, e) $n = 1$ and (c, f) $n = 2$. Vacuum level, Fermi level, and CBM are indicated by red, blue and green lines in electrostatic potential distributions, respectively.

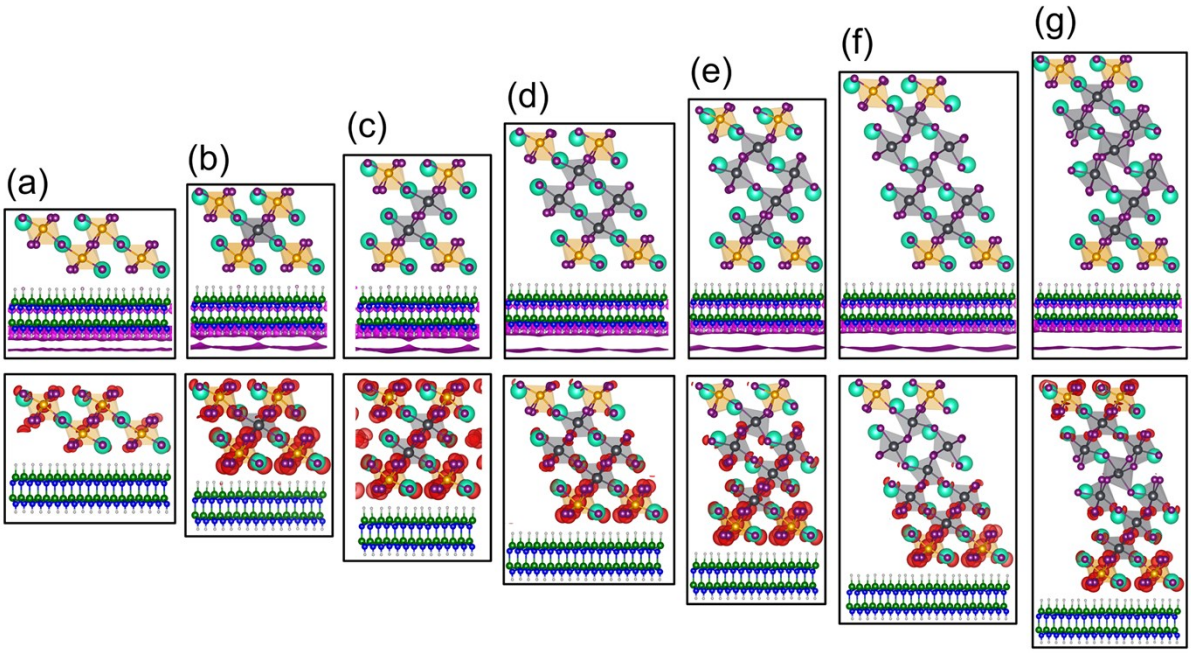

Fig. S13. Charge-density distributions of CBM (upper panels) and VBM (lower panels) of $Cs_{3+n}Pb_nSb_2I_{9+3n}$ /GaN heterostructures with (a) n = 0, (b) n = 1, (c) n = 2, (d) n = 3, (e) n = 4, (f) n = 5 and (g) n = 6, respectively.

Section S12. The comparison of PCE among existing heterostructures

Table S7. Confirmed existing heterostructures and their PCE (SLME) measured under the global AM1.5 spectrum (1000 W m^{-2}).

Classification	PCE (%)	References	Years
$Cs_{3+n}Pb_nSb_2I_{9+3n}$/GaN	**5.1~28.5**	**This work**	**2019**
Cu_4O_3 film	2.25	[6]	2019
AsP/CdSe heterostructure	13	[7]	2019
2D perovskite homologous	4.4~6.9	[8]	2017
$Zn_{1-x}Mg_xO$/$MAPbI_3$/Spiro-OMeTAD	16.5	[9]	2016
Cu-V-VI films	23~27	[10]	2013

REFERENCES

1 Z. Xiao, W. Meng, J. Wang, D. B. Mitzi and Y. Yan, *Mater. Horizons*, 2017, **4**, 206-216.

2 A. Swarnkar, A. R. Marshall, E. M. Sanehira, B. D. Chernomordik, D. T. Moore, J. A. Christians, T. Chakrabarti and J. M. Luther, *Science*, 2016, **354**, 92-95.

3 M. E. Levinshtein, S. L. Rumyantsev and M. S. Shur, *Properties of Advanced Semiconductor Materials: GaN, AIN, InN, BN, SiC, SiGe*, John Wiley & Sons: U.K., 2001, p2.

4 H. A. Elhamid, Y. Ismail and M. Deen, *Opt. Quant. Electron.*, 2013, **45**, 885-899.

5 Z. J. Wu, E. J. Zhao, H. P. Xiang, X. F. Hao, X. J. Liu and J. Meng, *Phys. Rev. B*, 2007**, 76**, 054115.

6. A. Živković, A. Roldan and N. H. de Leeuw, *Phys. Rev. B*, 2019, **99**, 035154.

7. X. Cai, Y. Chen, B. Sun, J. Chen, H. Wang, Y. Ni, L. Tao, H. Wang, S. Zhu and X. Li, *Nanoscale*, 2019, **11**, 8260-8269.

8 J. Qian, Q. Guo, L. Liu, B. Xu and W. Tian, *J. Mater. Chem. A*, 2017, **5**, 16786-16795.

9. J. Song, E. Zheng, L. Liu, X. F. Wang, G. Chen, W. Tian and T. Miyasaka, *ChemSusChem*, 2016, **9**, 2640-2647.

10. L. Yu, R. S. Kokenyesi, D. A. Keszler and A. Zunger, *Adv. Energy Mater.*, 2013, 3, 43-48.